Int. J. Heat Mass Transfer, Vol. 25, No. 1, pp. 99–110, 1982.
Printed in Great Britain

0017–9310/82/010099–12 $03.00/0
Pergamon Press Ltd.

CHARACTERISTICS OF INCLINED THIN FILMS, WAVINESS AND THE ASSOCIATED MASS TRANSFER

NEIMA BRAUNER and DAVID MOALEM MARON
School of Engineering, Department of Fluid Mechanics and Heat Transfer, Tel-Aviv University, Tel-Aviv, Israel

(*Received* 5 *January* 1981 *and in revised form* 29 *June* 1981)

Abstract—The relationship between the undulatory nature of inclined thin film flows and the transfer characteristics have been demonstrated and qualitatively established. This provides a basis for future analytical treatments of the hydrodynamics of wavy flows and their influence on the transport phenomena.

The boundary between the smooth film entry region and the wavy region has been discussed with relation to various operation conditions. The waviness characteristics at the rippled region and their development have been broadly studied and discussed.

NOMENCLATURE

f, wave frequency [s^{-1}];
G, power spectral density function [m^2];
g, gravity acceleration [m/s^2];
h, local film thickness [m];
$h_{\alpha,}$ Nusselt film thickness [m];
k_m, mass transfer coefficient [m/s];
l, spacing between probes [m];
L_i, wave inception distance [m];
R, correlation function [m^2];
Re_N, film Reynolds number;
t, time [s];
$\bar{U}_N$, Nusselt average film velocity [m/s];
V, voltage signals;
V_w, wave velocity [m/s];
X, downstream distance [m].

Greek symbols

α, inclination angle;
Γ, liquid feed rate (per unit width) [kg/s m];
θ, phase angle;
μ, liquid viscosity [kg/s m];
ρ, liquid density [kg/m^3];
σ, liquid surface tension [N/m];
τ, time shift [s].

INTRODUCTION

FLUID motion and transport in thin free surface liquid films are of fundamental interest in basic industrial equipment, e.g. in steam condensers, wetted wall columns, liquid film evaporators and other processes involving interfacial heat and mass transfer. The increased rates of transfer of momentum [1], heat [2–5] and mass [6–12], in both liquid and (the adjacent) gas phases, are usually related to the wavy nature of the film flow.

However, it is interesting to note that some inconsistencies seem to appear in the literature. For instance, mass transfer measurements at the solid–liquid boundary of a falling film did not demonstrate a pronounced wave action [16–19], apparently because short transfer surfaces (up to 10 cm) were used. On the other hand, waves induced by intermittent liquid feed (as in film flow over horizontal tube bundle) were found to enhance the mass transfer rate by a factor of two as compared to smooth continuous film flow[20].

The enhancement in the transfer rates, whenever it appeared, has been firstly attributed to an increase in the interfacial area. Recent studies imply that other mechanisms (such as local mixing, surface renewal or convective motions), which are induced by the undulatory character of the flow, may strongly contribute to the enhanced transfer rates [12–15]. However, the lack of transfer characteristics under controlled hydrodynamic conditions does not allow a comprehensive interpretation of the basic interactions between the waviness and the associated transport phenomena. Moreover, the available experimental data of transfer rates in wavy flow usually considers the overall rate, which integrates transfer behaviour in the smooth entry region, in the region where waves develop as well as in the region where fully developed wavy flow is established. Thus, it is expected that simultaneous observations of the local instantaneous transfer process and the sweeping hydrodynamic wave may enlighten some basic conceptions on the interactions between the two phenomena.

It is the purpose of the present project to establish the relationship between the waviness characteristics and the associated transport processes. The first phase presented here is aimed to demonstrate the hydrodynamic and transfer characteristics under a wide range of well controlled conditions and thus, to provide basic thoughts on the mechanism by which the waves are built-up, hence on the mechanism of transport in wavy flows. Secondly, to define those regions which are to be considered as of wavy nature and

thirdly, to determine the waviness characteristics in these wavy regions.

THE EXPERIMENTAL SET-UP

General

Consistent with the main objectives stated earlier an experimental set-up has been designed and constructed to provide comprehensive observations of the transport and the waviness characteristics in thin films. As the interactions between the waviness characteristics and the transport is of a central importance in the present study, a requirement has been put on taking the observations simultaneously at various points downstream.

Instantaneous local transfer rates between falling liquid film and an inclined plate are measured by the well known electrochemical technique [21]. The electrochemical process used here is the chemical reduction of ferricyanide ions, $Fe(CN_6)^{-3}$, at a nickel cathode and formation of a ferrocyanide ions $Fe(CN_6)^{-4}$. The reaction at the anode surface is the reverse one. At the limiting current (where the chemical polarisation is negligible), the current flowing in the electrochemical cell is independent of the applied potential and is governed by the availability of the ferricyanide ions from the bulk solution to the cathode surface. That is to say, ferricyanide ions, originating from the bulk, immediately react at the surface and the concentration of ferricyanide ions at the cathode surface is made negligible compared with the bulk concentration.

In general, the rate of transfer at the solid–liquid boundary is expressed in terms of the (electrical) migration, molecular diffusion and forced convection. The migration effect can be neutralized by adding a large excess of an unreactive electrolyte (NaOH) to the solution. In addition to that, if the conductivity of the inert electrolyte is high compared to that of the reacting species, the ohmic resistance of the whole solution is negligible, hence a sharp drop of electrical potential near the electrode is avoided. Under such conditions the measured transfer rates are mainly due to the diffusion and convection. However, for thin films, where the net bulk flows perpendicular to the transfer surface is sufficiently small, the contribution to the transfer process is mainly due to diffusion.

Local instantaneous film thickness measurements are recorded in parallel and simultaneously with mass transfer measurements by the capacitance method [22, 23]. An air condenser is formed by the combination of the wetted test plate and a small probe facing it (since the liquid film is of an electrolytic solution). The external probe is set into a non-conducting external flexiglass frame, driven by a travelling screw arrangement. The capacitance of the air condenser follows the variations in the thickness of the gap of air between the plate and the external probe, which in turn results from the variations in the film thickness.

The electrical devices of measurements will be further detailed below. First, a general description of the flow system is given.

The flow system

The flow system, shown schematically in Fig. 1, consists of the test tunnel and the feeding cycles.

The test tunnel, made of Plexiglas, is connected to a feeding chamber on one side and to a collector chamber on the other side. It is set on a heavy concrete table, which provides the possibility to change the tunnel inclination. The test plate lies on the bottom of the tunnel and is in fact a Printed Circuit Board (PCB), 63 cm width and 120 cm length. It is made of a nickel plate copper film and comprises the anodes, the control cathode and the test electrodes. The various electrodes are electrically isolated from each other. The control cathode is a 2.5 cm wide strip, located at the center of the plate and is used to provide overall transfer rates (space averaged coefficient) associated with various modes of film flow. The test electrodes, 1.2 mm nickel plated brass pins, are set at different distances along the control cathode flush with the upper surface of the plate, so that local mass fluxes can be measured. There are 44 test electrodes with gradually increasing spacing in the flow direction. The remaining plate area, at both sides of the control cathode, serve as anode surfaces, which are of 25 times larger surface area compared to the cathode surface. The control cathode and the test electrodes are electrically connected through power supply system to the anode sections and the whole circuit is closed through the liquid film.

The liquid employed in the experiments is an equimolar solution 0.01 M potassium ferricyanide and 0.01 M potassium ferrocyanide in a 1 M solution of sodium hydroxide in distilled water. The physical properties of the solution are determined according to the sodium hydroxide concentration and the temperature of the solution.* As the solution is a highly corrosive one, the whole flow system is made of non-corrosive as well as electrically inert materials. The electrolyte solution is recirculated through ducts of p.v.c. utilizing polypropylene pumps, leading from the storage tank to a constant level reservoir. The solution flows under gravity to the feed entry of the test tunnel and the flow rate is measured by a set of rotometers with nickel floats. A continuous feed is obtained by the liquid freely over-running an open feeding entry which extends over the whole width of the test tunnel. The liquid is recovered through a perforated collector chamber at the end of the tunnel, back to the storage tank.

The electrical devices

A detailed description of the electrical devices and instrumentation is given by the authors elsewhere [24]. Here, only a general scheme of the electrical

* The molecular viscosity is 1.2 cp and the surface tension is 10 dynes/cm.

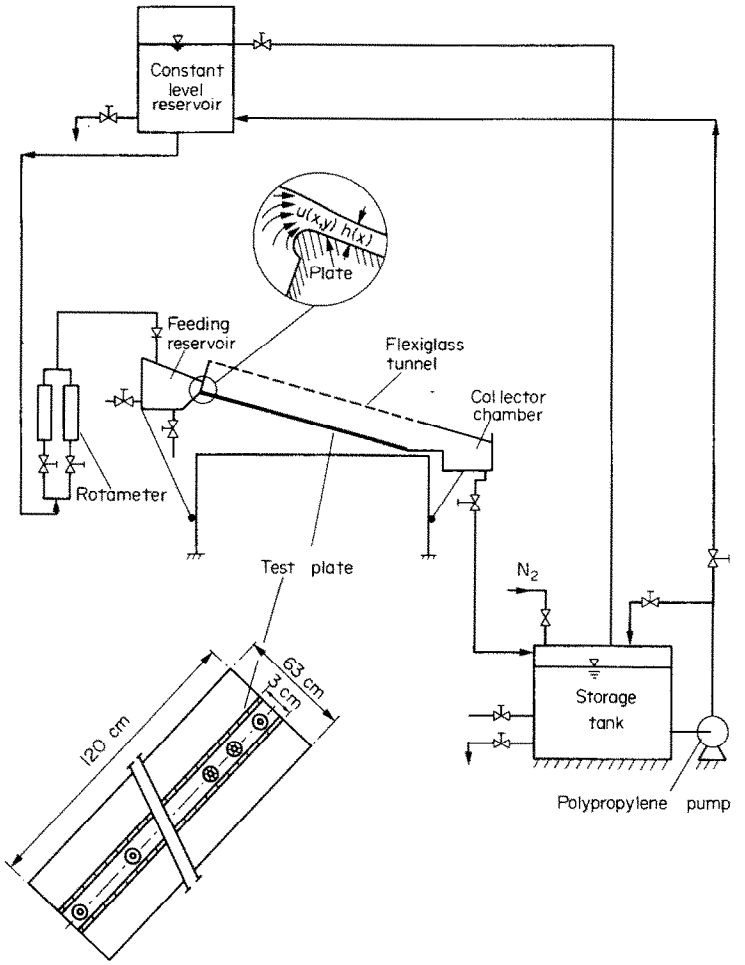

FIG. 1. Schematic representation of flow system.

measurements circuits is presented in Fig. 2. The positive poles of two power supply systems are connected to the anode sections. The negative pole of power supply (1) is connected to the control electrode, and the negative pole of power supply (2) is connected to a test electrode. The flow conditions are set first and then the limiting current is found by increasing the voltage of power supply (1) in small increments and measuring the electric current through the control electrode by reading the voltage drop over R_2 resistance. Then, the variable power supply (1) is set to the desired voltage in the limiting current range.

Space averaged mass transfer coefficient can be measured by recording the voltage drop over R_2 resistance. The local mass transfer coefficients can be measured simultaneously at six test electrodes (all other test electrodes are shorted to the control electrode). Measurement selector switch A connects the DMM (Digital Multimeter) to one of the measured channels. The DMM is balanced by varying R_0 resistance so that an equal potential drop over the control electrode and the measured test electrode is achieved. The electrical current which passes through the test electrode is measured indirectly by measuring the voltage drop over R_1 resistance and is utilized to evaluate the mass transfer rate to the electrode surface. The voltage output is connected through NEFF 124A amplifier to a data acquisition system.

In order to enable simultaneous measurement of local mass transfer coefficients and local film thickness, special arrangements in the electric circuit are required. The electric current in the local mass transfer measurement circuit is only a few microampers, thus a high amplification rate is required. On the other hand, the variations in the capacitance to be measured are in the range of 0.05–0.1 pF. The sensitivity of the capacitometer (Model 72B of Boonton Electronics Co.) is achieved by producing 1 MHz signal. This high frequency signal is applied simultaneously to both input terminals of the differential amplifier (common-mode signal). The RF (radio frequency) common mode signal is rectified in the amplifier and produces a d.c. output, which makes the mass transfer measurement impossible. Thus, it was necessary to include 1 MHz blocking filter in the electric circuit [24].

Another problem that arises from the interaction

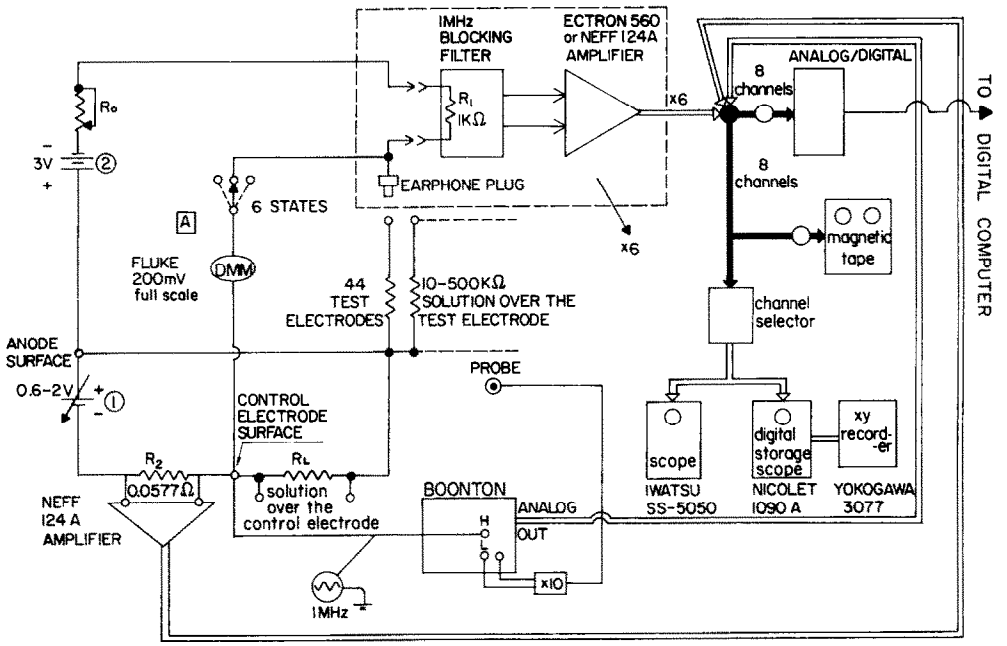

FIG. 2. Essential representation of the electronic systems.

between the mass transfer and capacitance circuits concerns the power supply systems to be used in the electrochemical circuit. A regular power supply system, which is operated from regular power line has parasitic capacitors to the ground. The impedance of these capacitors at 1 MHz is much smaller (about 1/1000) than the impedance of the coil in the capacitance meter at 1 MHz. Thus by using a regular power supply system, the 1 MHz signal of the capacitometer is practically shorted. It was necessary to build a special power supply system based on rechargable batteries. A schematic representation of the power supply system and the blocking filter is detailed elsewhere [24].

The output signals from mass transfer and capacitance measurements are transferred to a Variaian 72 digital computer for sampling and analyzing the collected data. This is done either by on-line sampling or by recording the analog output signals on a magnetic tape recorder/reproducer (Honeywell, model 5600C which is capable of recording/reproducing up to 14 channels simultaneously) and sampling by the computer later on.

RESULTS AND DISCUSSION

One of the advantages of the present experimental set-up is in providing simultaneous observations of the film thickness and the transfer rate at a point all along the undeveloped as well as the developed regions.

A typical time-trace records of the local instantaneous transfer rate with the simultaneously sweeping hydrodynamic wave (at the same point) are demonstrated in Fig. 3. Each pair of records represents the film thickness and the transfer rate obtained at a 90 cm distance downstream the top of the surface. The angle of inclination is 30°, in which case, well developed waves are already obtained at this distance [25]. As is shown in the figure, a periodic nature is also established for the mass transfer rates as a result of the hydrodynamic waviness.

Inspection of Fig. 3 indicates a few points worth mentioning. The first is that the fluctuations in the transfer rates are directly related to the hydrodynamics periodicity and the more intense the wavy nature of the flow, the more the transfer fluctuations are intensified. This is practically so for low Reynolds numbers. For the higher range of Reynolds number, only mild increase in the transfer fluctuations does result, though the disturbances in the film thickness continue to grow with the flow rate. This is understandable in view of the fact that the transfer process takes place at the solid–liquid interface. Hence, increasing the waviness at high liquid flow rates not necessarily enlarge its effect deep enough into the liquid film, close to the solid boundary. For a similar reason, the small waves, which cover the substrate film, separating two adjacent large waves (and the large waves) are of negligible or no effect on the solid–liquid transfer rates. However, it is expected that for different transfer processes, taking place at the liquid free interface, one could comfortably speculate that both types of waves may contribute to the interfacial transport characteristics.

Another point of interest to be noted in view of Fig. 3 is the phase relationships between the film waviness and its associated transfer rates. A careful observation of an h–k pair record reveals a rise in the transfer rate starting just ahead of the moving wave front. The

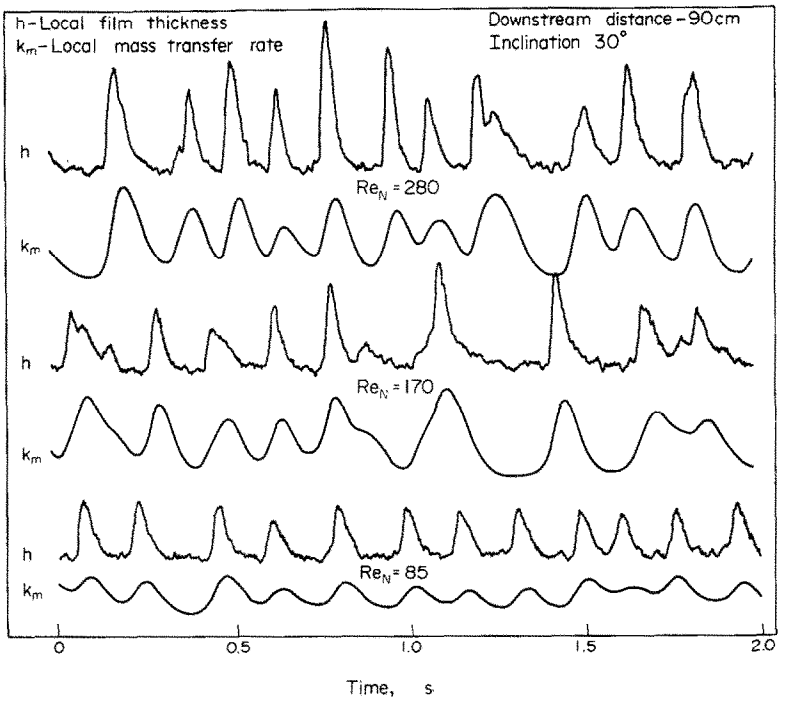

FIG. 3. Simultaneous time traces of local instantaneous film thickness and transfer rate.

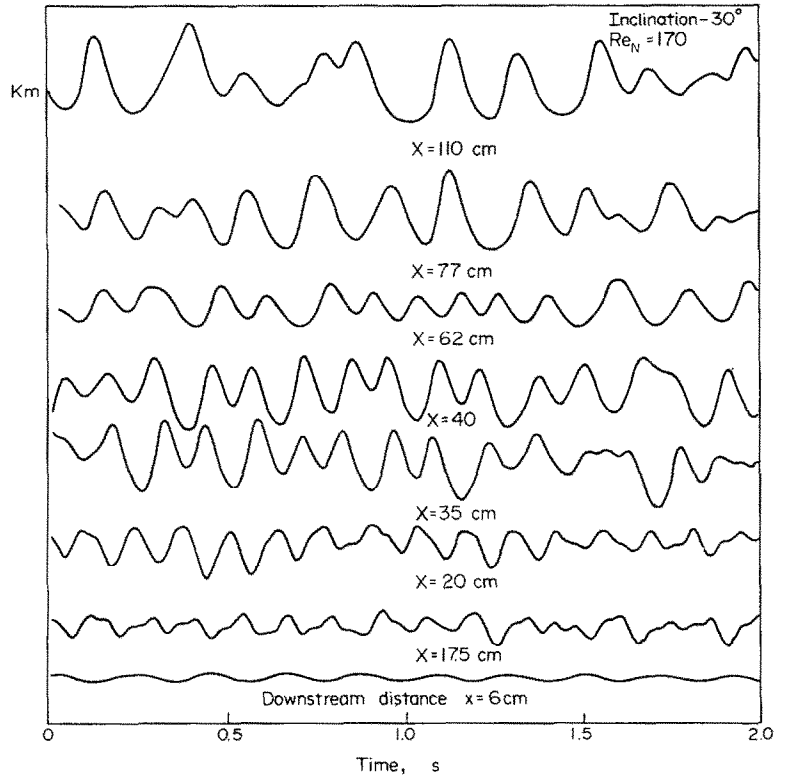

FIG. 4. Local instantaneous mass transfer records at various distances downstream.

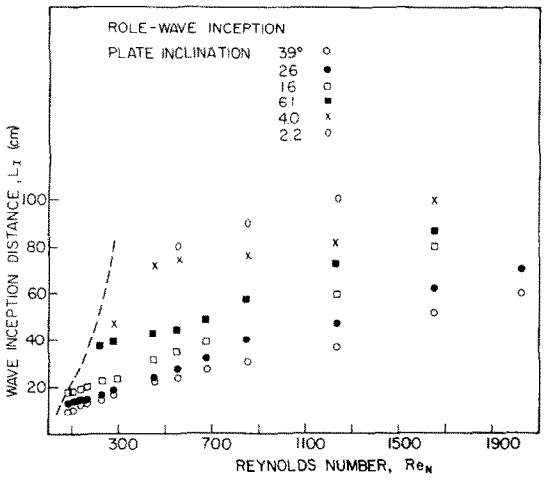

FIG. 5. Wave inception distance for various degrees of inclination and various liquid Reynolds numbers.

transfer rate continuously increases as the wave front is passing by, reaching its maximum value just beyond the wave peak. Thus, the peak of the transfer rate is somewhat lagging the peak region of the hydrodynamic wave. However, the major increase in the transfer rate occurs in the wave front region. At the wave trail a decay in the transfer rate takes place which seems to end at the thin substrate film just ahead of the next front where the transfer rate is periodically recovered.

The relationship between film waviness and the mass transfer characteristics is reinforced by similar time traces at the undeveloped region where the initially smooth film is firstly disturbed by shallow interfacial high frequency ripples. These short waves, being sufficiently dense at the inception region, overlap one another and thus generate larger lumps of liquid downstream with lower frequency and higher translational velocity, until steady-periodic roll waves develop. The latter, due to their deep penetration into the liquid film, have a well pronounced influence upon the

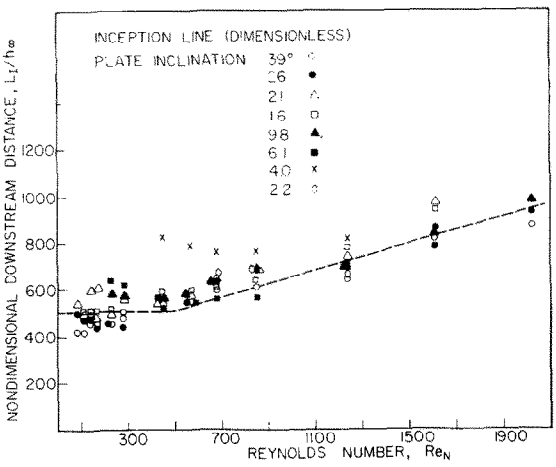

FIG. 6. Non-dimensional downstream distance of wave inception.

transfer process, which is further intensified due to the thickening of the mass boundary layer downstream. However, it is to be noted that the effect of the undulatory nature of the interface on the transfer already exists on the underdeveloped region, where the ripples are shallow and the boundary layer relatively thin.

It is interesting to refer here to the simultaneous recordings of wall shear stress and roll wave profiles taken by Hanratty *et al.* [26] in horizontal cocurrent gas–liquid flow. A sudden relaxation of the wall shear stress in the wave front has been noticed whereby the stress in the front region decreases to a value which is lower than the stress excited by the substrate ahead. At the peak region of the wave, a steep increase in the stress takes place, followed by a gradual decrease in the wave trail. The sudden relaxation of the shear stress of the wave front and the above-mentioned steep increase in the transfer rate implies that a renewal phenomenon characterizes the mechanisms associated with the wave front. Thus the above observations on the interactions between the hydrodynamic and the transport characteristics, though rather qualitative, are of a great importance in establishing basic thoughts on the transport mechanism taking place. Moreover, local instantaneous observations of the transfer rates may lead to some conceptions on the basic processes of build-up and shedding of these lumps of liquid associated with kinematic wave. Indeed, such routes for modelling the kinematic waves in thin film flow and for prediction of the resulting transport characteristics are presently underway by the authors.

As it is pointed out in Fig. 4, a wave-free entry region exists beyond which a gradual development of wave motion sets in. This distance is referred to as the wave inception line, and is encountered in the literature usually via studies on the stability of falling liquid films. However, most of the studies which relate to this concept deal with vertical films of relatively low liquid flow rates (Re_N up to 100). A comprehensive study on the onset of waves (including minimum rate for complete wettability and break-up of thin film etc.) is presented by the authors elsewhere [25]. However, included here are some representative results on the inception, those which contribute to the understanding of the transport phenomena at the various flow regimes. Figure 5 represents the wave inception distance for various degrees of inclination and over a wide range of liquid flow rates. The lower limit of Re_N was determined by the minimum flow rate required for uniformly wetting the plate surface. As is expected, increasing the liquid rates yields an extended ripple-free entry region, while for relatively low rates associated with thin films, the onset of waves is more easily developed. Also it is shown in Fig. 5 that for small degree of inclination the wave inception is significantly delayed. For instance, for the particular plate used here (120 cm in length) no ripples are practically visible at 2° (except for lower range of Reynolds numbers).

As stability analysis shows, the critical Reynolds number where stable, smooth laminar film can still prevail, decreases with the inclination and approaches zero for vertical films. Here, however, except for the lower inclination (of 2–4°) the critical Reynolds number is lower than that required for fully wetted surface. The latter is shown by the broken line in Fig. 5. From the practiced point of view, fully wetted surfaces can be considered wavy except for an inclination lower than 2°.

It is interesting to note that normalizing the inception distance for the various conditions in Fig. 5 by the corresponding Nusselt film thickness (at the appropriate inclination) as shown in Fig. 6, yields a somewhat universal correlation between the dimensionless inception distance with Reynolds number:

$$L_i = 500h_\infty, \quad Re_N < 500,$$

$$L_i = (350 + 0.03\,Re_N)h_\infty, \quad Re_N > 500,$$

$$h_\infty = \frac{1}{3}\left[\frac{3}{4}\frac{\mu^2 Re_N}{\rho^2 g \sin\alpha}\right],$$

where L_i is the inception distance, h_∞ is the Nusselt film thickness corresponding to a Reynolds number given by $4\Gamma/\mu$ (Γ is the liquid feed rate per unit width, α is the inclination to the horizontal and ρ, μ are the density and viscosity of the liquid, respectively).

Note also that the scattering in Fig. 6 should not underrate the generality of the correlation in as much the characteristic length used for normalization is much smaller than the average inception distance. Moreover, the initial inception of waves is sensitive to the moe of liquid distribution and to any contingent disturbances. Therefore, the results in Figs. 5 and 6 may be assumed fairly representative for similar systems in estimating the boundary between the entry region and the wave-controlled region.

Consistent with the objectives stated earlier, the emphasis in the present study is more on the appearance of those waves which affect the transport characteristics. For thin films (and in view of the time traces in Fig. 3 and 4), the appearance of roll waves is of immediate influence of the transfer at the other boundary. Thus, the presence of the effective roll waves can easily be determined from the instantaneous transfer rate traces. This is demonstrated in Fig. 7 where the relative fluctuations over the time average value is presented along the entire plate length, covering both sides of the inception. Note that since the inception for $Re_N <$ 1000 is weakly dependent upon Re_N, the inception for the range considered in Fig. 7 is given by a point, $x/h_\infty \approx 500$. It is also indicated in the figure that the relative fluctuations of the local mass transfer coeffieients increase in the downstream direction even after the region of well developed waves is reached as a result of the continuously decreasing values of the local time-averaged transfer rate.

A representative comparison of the relative fluctuations for nearly horizontal and inclined flow is demonstrated in Fig. 8 for an intermediate Reynolds number. Again since the wave inception distance for low inclination is practically out of the confines of the plate, very moderate fluctuations are noticed at 2° of inclination. It is worth noting that the fluctuations in Fig. 8 are normalized with reference to local time averaged transfer rate in each case. However, since the time averaged for 30° is greater (twice) than that of 2°, the ratio of the absolute fluctuations is even higher than that indicated in the figure.

Having demonstrated the close relationship between the transport phenomena and the interfacial waviness, two main questions are posed: (a) What are the waviness characteristics for various operation conditions and (b) to what extent are the transfer rates intensified (whether they are) due to these characteristics? The second question will be dealt with

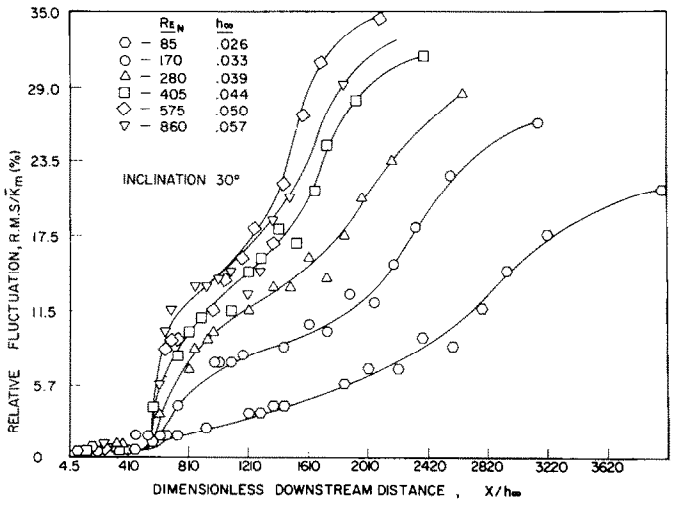

FIG. 7. Variations of relative fluctuation of local mass transfer coefficient (R.M.S/$\bar{k}_m$) with the distance downstream.

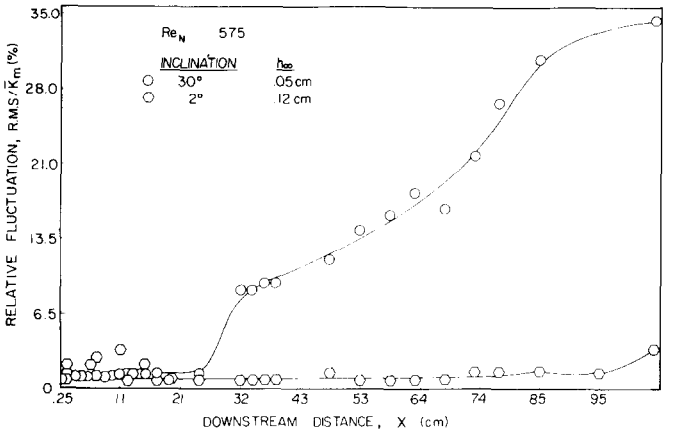

FIG. 8. Effect of inclination on the relative fluctuation of the transfer rate along the plate.

in a presentation to come. This discussion continues by presenting the characteristics of the wavy nature of the flow.

Waves are characterized by their frequency, translational velocity and wave profile, which depend upon the film Reynolds number, plate inclination and downstream position. The waves are first initiated at the wave inception region, change shape while moving downstream and thus develop into large solitary waves which are preceded by a train of ripples covering the thin substrate. However, these secondary waves (in contradistinction from the small waves in the inception region which originate the roll waves downstream) are of no effect on the transport (as discussed with respect to Figs. 3 and 4) and thus the information obtained from the transfer measurements is due to the large waves characteristics only. The availability of simultaneous information of instantaneous mass transfer rates at several locations provides a very convenient way for evaluating the development of these characteristics downstream. Considering that the wavy flow has a stochastic nature, the data processing involves the usual techniques for analyzing stochastic processes, namely sampling and evaluating the power spectral and cross-spectral densities of the obtained information. Assuming the process to be stationary and ergodic, the auto- and cross-correlation functions of two simultaneous signals $V_i(t)$, $i = 1, 2$, are given by the expressions:

$$R_{ii}(\tau) = \lim_{T\to\infty} \frac{1}{2T} \int_{-T}^{T} V_i(t)\, V_i(t+\tau)\, \mathrm{d}t$$

auto-correlation

(3)

$$R_{12}(\tau) = \lim_{T\to\infty} \frac{1}{2T} \int_{-T}^{T} V_1(t)\, V_2(t+\tau)\, \mathrm{d}t.$$

cross-correlation

Also, the auto-correlation and power spectral density functions are related by a Fourier transform as follows:

$$G_{ii}(f) = \int_{-\infty}^{\infty} R_{ii}(\tau)\, \mathrm{e}^{-i2\pi f\tau}\, \mathrm{d}\tau. \tag{4}$$

Similar relations exist between the cross-correlation and the cross-spectral density functions:

$$G_{12}(f) = \int_{-\infty}^{\infty} R_{12}(\tau)\, \mathrm{e}^{-i2\pi f\tau}\, \mathrm{d}\tau \tag{5}$$

where the phase angle is:

$$\theta_{12}(f) = \arctan\left\{\frac{\mathrm{Im}[G_{12(f)}]}{\mathrm{Re}[G_{12(f)}]}\right\}. \tag{6}$$

The power spectral density function describes the general frequency composition of the data in terms of the spectral density of its mean square value (energy), while the cross-spectral density function is used to determine the time delay or velocity, required for the given signal to pass between the two measurement points. Hence, the time delay τ, the velocity Vw and the (known) spacing l between the probes are simply related by

$$\tau = \frac{\theta_{12(f)}}{2\pi f} = \frac{l}{Vw} \quad \text{or} \quad \theta_{12}(f) = \frac{2\pi l}{Vw} f \tag{7}$$

where $\theta_{12}(f)$ is given by equation (6). Equation (7) implies that the velocity of a wave with a given frequency can be derived from the slope of the phase angle as a function of frequency.

Typical spectral and cross-spectral densities of the local voltage signals (obtained after eliminating the d.c. component) from electrodes located at various distances downstream are shown in Fig. 9. At a distance of 90 cm, Fig. 9(c), the wave spectrum displays one clear maximum at a frequency of about 5 Hz. The fact that the spectrum density of two probes (spaced 7.5 cm) and their cross-spectral density are almost identical indicates that the waves preserve their shape between these two measurement stations, and that over this spacing distance, the process can be considered stationary with respect to position. However, it seems that the frequency of 5 cycles shown in Fig. 9(c)

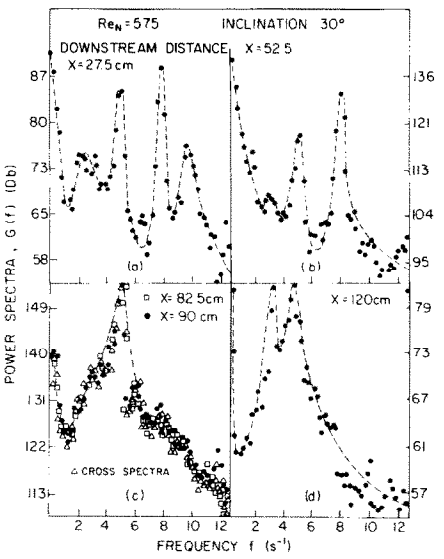

FIG. 9. Power spectral density of mass transfer fluctuation at various locations downstream [including cross-spectra in (c)].

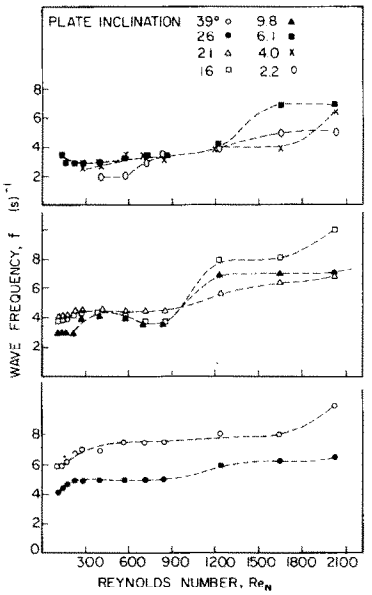

FIG. 10. Downstream frequency for various Reynolds numbers and various degrees of inclination (at $x = 100$ cm).

is not yet the fully developed one. This is in view of Fig. 9(d) where a lower frequency component of 3 cycles is being built-up. Note that the spectrum of Fig. 9(d) is obtained by inserting the control electrode and processing the average transfer rate signal. The latter obviously reflects the periodicity of the last wave front leaving the transferring surface where the dominant frequency is still 5 cycles. This frequency is reflected at other points upstream due to the fact that the whole film covering the surface is a part of the electronic measurement circuit.

The development of the characteristic frequency can be followed by inspection of the spectral density spectrums of earlier points upstream as in Figs. 9(a, b). The spectrum in Fig. 9(a) corresponds to an electrode located at the inception line. It indicates high frequency components (8 cycles or even higher) which correspond to the preliminary waves originating at the inception. At a further distance, as Fig. 9(b) shows, the highest frequency component is the first to disappear, since the process of overlapping between the high frequency waves is the first to occur. The reduction in the frequency continues until steady waves are obtained.

Figure 10 represents wave frequency at 100 cm downstream for various Reynolds numbers and plate inclinations. For the low range of Reynolds numbers, the frequency shows a mild dependence upon the Reynolds number. The increase in the wave frequency at higher Reynolds numbers is as a result of the movement of the inception region towards the measurement point (at 100 cm). The effect of the inclination on the other hand, is two-fold: in general, decreasing the inclination results in lower frequency. In parallel, the inception for low inclination moves downstream and this affects higher frequencies at the measurement point. Depending upon the liquid rates and inclination these opposing effects might compensate each other as is shown in Fig. 10. It is only parenthetically noted here that the equilibrium frequencies for continuous liquid feed remain unchanged with equivalent intermittent feed [28]. The effect of liquid distribution is thus limited to the underdeveloped region. This fact is of a high importance in modelling the wave characteristics at the developed region.

As equation (7) implies, the translational wave velocity is obtained by plotting the phase angle as a function of frequency. A typical plot, corresponding to Fig. 9(c), is presented in Fig. 11. The slope yields the average velocity of waves passing the pair of probes which provide the cross-spectral density data.

Figure 12 represents the wave velocity for various films Reynolds numbers and inclinations. Generally, the final steady velocity is higher than that of the undeveloped region. The distance required to achieve steady velocities depends, among other things, upon the location of the inception region. High inclinations and low liquid flow rates are associated with earlier waves inception and thus the steady wave characteristics are approached faster.

The 'steady' wave velocity at the well developed region for the inclination of Fig. 12 and over a wider range of Reynolds number has been normalized with reference to the corresponding average Nusselts velocity and is presented in Fig. 13. A general trend of decreasing celerity with Reynolds number is indicated. The major reduction occurs in the range of $Re_N < 600$, where for sufficiently high Reynolds number the celerity approaches a value 1.50. This asymptotic value has been already reported for vertical wavy flows.

FINAL REMARKS

A number of conclusive remarks are to be noted:

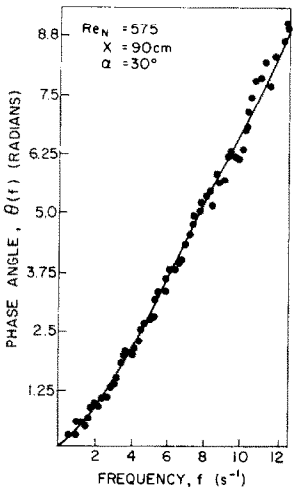

FIG. 11. Phase angle variation with the frequency.

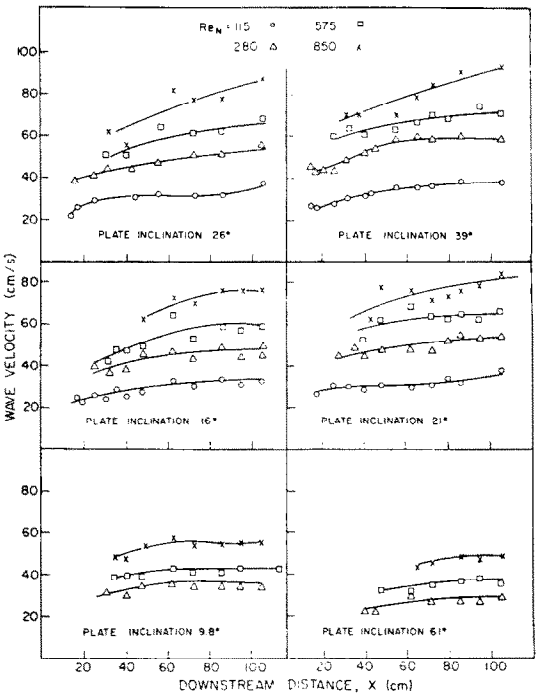

FIG. 12. Wave velocity at various Reynolds numbers and various degrees of inclination.

(a) The boundary between the smooth entry region and the rippled wavy one is proportional to the steady Nusselt film thickness, h_γ. Thus, it is proportional to the cubic root of the liquid flow rates and is inversely proportional to the cubic root of the inclination (sin α). For $Re_N > 500$, the proportionality is somewhat higher (see Fig. 6).

(b) At the inception region, dense waves are initiated at relatively high frequency. Lower frequency is indicated at the well developed region, which has a mild dependence upon the liquid rate and no dependence upon the mode of liquid feed distribution. This implies that the equilibrium frequency is an inherent quality, which relates to the characteristics of the flow at the well developed region and not of the upstream conditions.

(c) In parallel to the significant decrease in the wave frequency, the celerity shows a relatively small increase in the underdeveloped region. Consequently, it seems that it is the wave length that mainly compensates for the decrease in frequency.

(d) The relationships between the sweeping by hydrodynamic wave and the local instantaneous mass transfer rate implies that a renewal phenomenon characterizes the mechanisms associated with wavy flows. Only the large waves affect mass transfer characteristics (at the solid–liquid boundary), due to their deep penetration into the liquid film. This furnishes a basis for modelling the transport in wavy flows (presently undertaken).

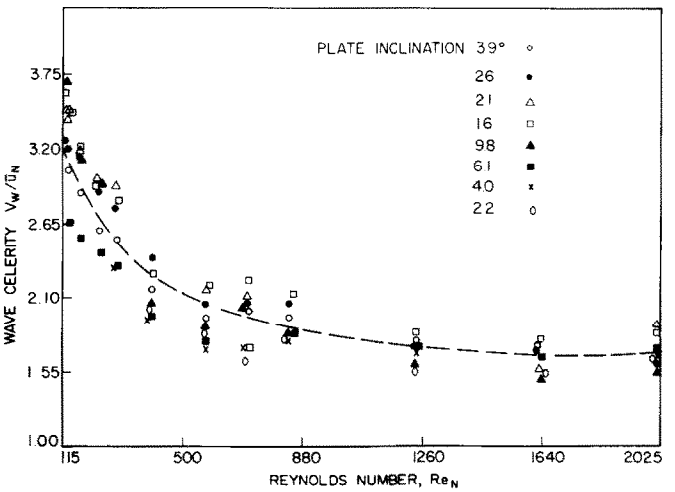

FIG. 13. Wave celerity (dimensionless) for various Reynolds numbers and various degrees of inclination.

Acknowledgement—We acknowledge with thanks the financial support of the Israel National Council for Research and Development and the sponsorship of the Israel Desalination Engineering Ltd., Tel-Baruch.

REFERENCES

1. A. E. Dukler, Characterization effects and modeling of the wavy gas–liquid interface, in *Progress in Heat and Mass Transfer*. Pergamon Press, New York (1972).
2. G. S. Bays and W. H. McAdams, Heat transfer coefficients in falling film heaters, *Ind. Engng Chem.* **29**, 1240–1246 (1937).
3. A. G. Williams, S. S. Nandapurkar and F. A. Holland, A review of methods for enhancing heat transfer rates in surface condensers, *Chem. Engng* **223**, CE367–CE373 (1968).
4. R. Chand and H. F. Rosson, Local heat flux to water film flowing down a vertical surface, *I/EC Fundamentals* **4**, 356–359 (1965).
5. I. M. Fedotkin and V. R. Firisyuk, Heat transfer rate along a surface wetted by a thin liquid film, *Heat Transfer Soviet Res.* **1**, 115–122 (1969).
6. R. E. Emmert and R. L. Pigford, A study of gas absorption in falling liquid films, *Chem. Engng Prog.* **50**(2), 87–93 (1954).
7. W. Brotz, Über die Vorausberechnung der Absorptionsgeschwindigkeit von Gasen in Strömenden Flüssigkeitsschichten, *Chem.-Ing.-Tech.* **26**, 470–478 (1954).
8. S. Kamei and J. Oishi. Mass and heat transfer in a falling liquid of wetted wall tower, *Mem. Fac. Engng Kyoto Univ.* **17**, 227–239 (1955).
9. D. P. Boyd and J. M. Marchello, Role of films and waves on gas absorption, *Chem. Eng. Sci.* **21**, 769–776 (1966).
10. J. C. Jepsen, O. K. Crosser and R. H. Perry, The effect of wave induced turbulence on the rate of absorption of gases in falling liquid films, *A.I.Ch.E.Jl* **12**, 186–192 (1966).
11. F. P. Stainthorp and G. J. Wild, Film flow—the simultaneous measurement of wave amplitude and the local mean concentration of a transferable component, *Chem. Engng Sci.* **22**, 701–704 (1967).
12. H. Brauer, Stoff-Austausch beim Rieselfilm, *Chem. Ing. Tech.* Nr. 2, **30**, 75 (1958).
13. G. D. Fulford, The flow of liquids in thin films, *Advances in Chemical Engineering* (Edited by Drew, Hooper and Vermeulen) Vol. 5, p. 151. Academic Press, N.Y. (1964).
14. S. Portalski and A. J. Clegg, Interfacial area increase in rippled film flow on wetted wall columns, *Chem. Engng. Sci.* **26**, 773 (1971).
15. C. Stirba and D. M. Hurt, Turbulence in falling liquid films, *A.J.Ch.E.Jl* **1**, 178–184 (1955).
16. H. Kramers and P. J. Kreyger, Mass transfer between a flat surface and a falling liquid film, *Chem. Engng. Sci.* **6**, 42–48 (1956).
17. D. R. Oliver and T. E. Atherinos, Mass transfer to liquid-films on an inclined plane, *Chem. Engng Sci.* **23**, 525–536 (1968).
18. A. Iribarne, A. D. Gosman and D. B. Spalding, A theoretical and experimental investigation of diffusion-controlled electrolytic mass transfer between a falling liquid film and a wall, *Int. J. Heat Mass Transfer* **10**, 1661–1676 (1967).
19. A. A. Wragg, P. Serapimidis and E. Einarsson, Mass transfer between a falling liquid and a plane vertical surface, *Int. J. Heat Mass Transfer* **11**, 1287–1289 (1969).
20. S. Sideman, H. Horn and D. Moalem, Transparent characteristics of films flowing over horizontal smooth tubes, *Int. J. Heat Mass Transfer* **21**, 285–294 (1978).
21. Mizushina, The electrochemical method in transparent phenomena, *Adv. Heat Transfer* **7**, p. 87 (1971).
22. A. E. Dukler and O. P. Bergelin, Characteristics of flow in falling liquid films, *Chem. Engng Prog.* **48**, 557 (1952).
23. S. R. Tailby and S. Portalski, The hydrodynamics of liquid films flowing on vertical surface, *Trans. Inst. chem. Engng* **38**, 324 (1960).
24. D. Moalem and N. Brauner, The effects of vapour flow and surface waves in improving the performance of water desalination units, Report No. 5, Tel-Aviv Univ. School of Engineering (March 1979).
25. D. Moalem Maron, G. Ingel and N. Brauner, Wettability, break-up and wave inception in inclined thin films with continuous and intermittent feed, to be submitted to the *Int. J. Heat Mass Transfer*.
26. M. Miya, D. E. Woodmanee and T. J. Hanratty, A model for roll waves in gas–liquid flow, *Chem. Engng Sci.* **26**, 1915–1931 (1971).
27. N. Brauner and D. Moalem Maron, Mass transfer in inclined thin films with intermittent feed, submitted to the *Chem. Engng Sci.*
28. N. Brauner and D. Moalem Maron, Modelling of wavy flow in inclined thin films, submitted to the *Int. J. Heat Mass Transfer*.

CARACTERISTIQUES DES FILMS MINCES INCLINES AVEC ONDES ET TRANSFERT MASSIQUE ASSOCIE

Résumé—La relation entre la nature ondulatoire des écoulements de film mince et les caractéristiques de transfert a été démontrée et qualitativement établie. Ceci fournit une base pour le traitement analytique futur de l'hydrodynamique des écoulements avec ondes et de l'influence de celles-ci sur le phénomène de transfert.

La frontière entre la région d'entrée de film lisse et la région ondée est discutée en relation avec des conditions variées d'opération. Les caractéristiques de la région avec rides et leur développement ont été largement étudiées et discutées.

EIGENSCHAFTEN GENEIGTER RIESELFILME, IHRE WELLIGKEIT UND DER DAMIT VERBUNDENE STOFFTRANSPORT

Zusammenfassung—Die Beziehung zwischen der welligen Beschaffenheit geneigter Rieselfilmströmungen und ihren Transporteigenschaften wurde nachgewiesen und qualitativ bestimmt. Damit ist eine Grundlage geschaffen für die künftige analytische Behandlung der Hydrodynamik welliger Strömungen und ihres Einflusses auf die Transportvorgänge. Die Grenze zwischen dem Einlaufbereich mit glattem Film und dem welligen Bereich wurde in Abhängigkeit von verschiedenen Betriebsbedingungen diskutiert. Die Eigenschaften der Welligkeit im Bereich der gekräuselten Filmoberfläche und ihre Entwicklung wurden ausführlich untersucht und besprochen.

ХАРАКТЕРИСТИКИ ТОНКИХ ПЛЕНОК НА НАКЛОННЫХ ПОВЕРХНОСТЯХ, ВОЛНИСТОСТЬ И СООТВЕТСТВУЮЩИЙ ПРОЦЕСС МАССОПЕРЕНОСА

Аннотация — Выявлена и качественно исследована связь между волнообразной природой стекания тонких пленок по наклонной поверхности и характеристиками переноса, что может служить основой для дальнейшего аналитического исследования гидродинамики волновых течений и их влияния на явления переноса.

Граница между начальным участком с гладкой пленкой и областью волнового течения рассматривается при различных рабочих режимах. Широко исследуются и анализируются характеристики волнового течения, начиная с области возникновения мелкой ряби.